Journal of Organometallic Chemistry 896 (2019) 24–31

Contents lists available at ScienceDirect

Journal of Organometallic Chemistry

journal homepage: www.elsevier.com/locate/jorganchem

Drastic effect of the substituent on the anthraquinone diimine moiety on the properties of the push-pull *trans*-bisphosphinebisphenylacetynylplatinum(II)-containing polymers

Frank Juvenal, Hu Lei, Paul-Ludovic Karsenti, Pierre D. Harvey*

Département de chimie, Université de Sherbrooke, Sherbrooke, PQ, J1K 2R1, Canada

ARTICLE INFO

Article history:
Received 2 March 2019
Received in revised form
25 May 2019
Accepted 25 May 2019
Available online 31 May 2019

Keywords:
Platinum(II)
Anthraquinone diimine
Polymer
Fluorescence
Transient absorption spectroscopy
2-Photon absorption

ABSTRACT

A new emissive polymer (**[Pt]**-(**AQI**$(OR)_2$))$_n$, **P2**, where **AQI** is anthraquinone diimine, **[Pt]** is *trans*-bis(ethynylbenzene)bis(tributylphosphine)platinum(II) and R is n-butyl, has been prepared in order to compare with the related polymer (**[Pt]**-(**AQI**$(NO_2)_2$))$_n$ **P1** (Macromolecular Chemistry and Physics (2018), 219(22), 1800354). In addition to the difference in substituent effect (electron donor, O-*n*-Bu; electron acceptor, NO_2), the first notable difference is the polymer dimension where the addition of soluble chains expectedly leads to longer polymer chains for **P2** (**P1**: $M_n = 88200$, $M_w = 188700$, $Đ = 2.14$, DP = 111; **P2**: $M_n = 147000$, $M_w = 327000$, $Đ = 2.23$, DP = 133). However, unexpected differences in photophysical properties exist despite their structural similarities. First, **P2** exhibits a higher fluorescence intensity and lifetime ($\tau_F \sim 1$ ns) with respect to that for **P1** ($\tau_F \sim 11$ ps), despite the fact that alkyl chains are known to deactivate excited states ("loose bolt effect"). Second, **P2** exhibits concurrently a rare case of higher energy fluorescence associated with an upper S_n excited state, which is not observed in **P1**. The two photon absorption properties of **P1** and **P2** have been acquired and both exhibit modest or similar cross sections ($53 < \sigma_2 < 89$ GM, **P1**; $45 < \sigma_2 < 70$ GM, **P2**; for laser power ranging from 252 to 327 GW/cm^2) in comparison with other [Pt]-containing polymers.

1. Introduction

Conjugated organometallic polymers of the type (**[Pt]**-**G**)$_n$ where the synthon **[Pt]** is *trans*-di(ethynyl)bis(trialkylphosphine) platinum(II) and **G** is a conjugated group, have attracted substantial attention over the past decades and were substantially reviewed [1–10]. The very recent advances include the preparation of chiral materials, whether they consist of atropisomers or enantiomers [11,12], or achiral ones [13–17]. In all cases the common denominator concerns photonics devices and their related properties (*i.e.* low band gap, light harvesting, emissive, electrochromic, and optical waveguiding materials), but this was not exclusive as catalytic activity was also reported for one case [18]. Concurrently over the past ten years, materials exhibiting nonlinear activities was also a subject of choice [19–24] along with the design of polymer light emitting diodes [25], but the design of organic solar cells was, and still is, the most investigated applications and properties for this synthon [26–35] and the field on their photovoltaic properties was recently reviewed [36,37] and **[Pt]**-materials attracted some attention in a theoretical stand point [38].

The highest photoconversion efficiency (PCE) reported so far is 5.29% for a bulk heterojunction solar cells containing the **[Pt]**-moiety [26,27]. It has been proposed that the use of the electron deficient anthraquinone, **AQ**, moiety should increase the PCE of (**[Pt]**-**G**)$_n$ materials in solar cells [28,31]. Our group has also designed an analogeous (**[Pt]**-**AQ**)$_n$ polymer where **AQ** = 2,6-anthraquinone, **P0** (Fig. 1), which turns out to be strongly phosphorescent at 77 K with an emission lifetime of ~270 μs. [39]. This (**[Pt]**-**AQ**)$_n$ structure differs from that where **AQ** = 2,7-anthraquinone, which only exhibits a fluorescence (with a lifetime in the ns time scale) [31]. Very recently, we designed another polymer using **G** = 2,6-substituted anthraquinone diimine, **P1** (Fig. 1) [40]. In this case, the polymer is weakly fluorescent at both 298 and 77 K, with fluorescence lifetimes in the order to 10–30 ps, with no evidence of phosphorescence. Such excited state lifetimes appear rather short and may prevent efficient electron transfer to occur. In addition, the structure-properties relationship appears rather difficult to pin down. The obvious structural modification is

* Corresponding author.
E-mail address: pierre.harvey@usherbrooke.ca (P.D. Harvey).

https://doi.org/10.1016/j.jorganchem.2019.05.024
0022-328X/

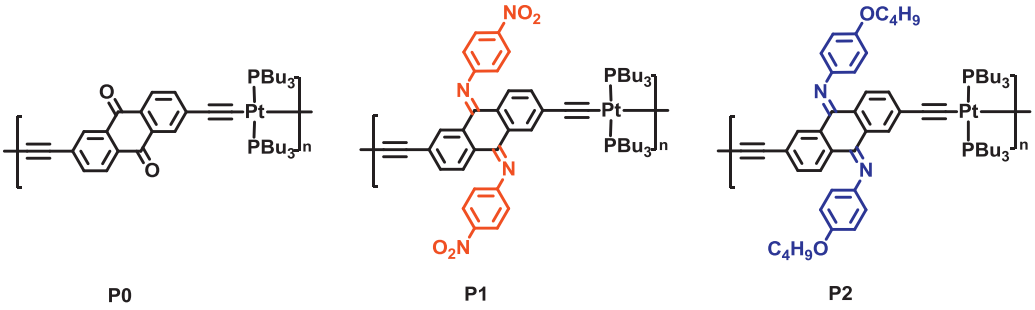

Fig. 1. Structures of **P0**, **P1** and **P2**.

to replace the electron withdrawing groups (NO_2) by electron donating (OBu). We now report the synthesis and characterization of **P2**, which a larger dimension compared to **P1** (expected), and a much longer S_1 excited state lifetime (unexpected).

2. Experimental section

2.1. Materials

The 2,6-bis(trimethylsilylethynyl)anthracene-9,10-dione [41] and *trans*-$Pt(PBu_3)_2Cl_2$ [42], were prepared according to literature procedures. Copper(I) iodide, tetrachlorotitanium(IV), 1,4-diazabicyclo[2.2.2]octane (Dabco), tributylphosphine, and 4-butoxyaniline were purchased from Aldrich and were used as received. Platinum(II) chloride was purchased from Alfa Aeser and used as received. All reactions were performed in Schlenk-tube flasks under purified argon. All flasks were dried under a flame to eliminate moisture. All solvents were distilled from appropriate drying agents.

2.1.1. N,N′-bis(4-n-butoxybenzene)(2,6-bis(trimethylsilylethynyl) anthraquinone diimine, *2a*

4-*n*-butoxyaniline (0.76 g, 4.0 mmol) and 1.35 g (12.0 mmol) of Dabco were dissolved in 25 mL of chlorobenzene while heating to 90 °C. Titanium tetrachloride (0.4 mL, 4.0 mmol) were then added dropwise, followed by the addition of 2,6-bis(trimethylsilylethynyl)-anthracene-9,10-dione (0.42 g, 2.0 mmol) and rinsing the powder addition funnel with 20 mL of chlorobenzene. The solution was stirred at 115 °C for 12 h. The product was isolated by filtering off the precipitate, washed with hot chlorobenzene (2 x 20 mL). The solution was evaporated. The solid was dissolved in $CHCl_3$, washed three times with water, dried with $MgSO_4$, and filtered. The $CHCl_3$ was completely evaporated leaving only the product. The product was purified on a silica column with $CHCl_3$ as the solvent to give compound **2a** as a red powder. (0.99 g, 90%). ^{1}H NMR (300 MHz, $CDCl_3$) δ 8.39 (d, $J = 1.4$ Hz, 1H), 8.26–7.58 (m, 1H), 7.23–7.14 (m, 2H), 7.07–7.01 (m, 2H), 6.95–6.83 (m, 8H), 4.06–3.86 (m, 4H), 1.89–1.68 (m, 4H), 1.59–1.40 (m, 4H), 1.13–0.92 (m, 6H), 0.36–0.11 (m, 17H). Mass spectrum: *m*/*z* (EI): 663.1847 (M^++Na^+).

2.1.2. N,N′-bis(4-n-butoxybenzene)(2,6-bis(ethynyl)anthraquinone diimine, *3a*

0.55 g (0.8 mmol) of **2a**, was placed in a 250 mL round-bottomed flask and 7 g of K_2CO_3 was added to the flask as well as 200 mL of a CH_3OH/THF (1:1) mixture. The reaction was stirred under Ar overnight until the solution turned orange. The excess K_2CO_3 was filtered and the remaining solvent was evaporated. The residue was dissolved in $CHCl_3$ and washed 3 times with water. The $CHCl_3$ solution was dried with K_2CO_3 and filtered. The product was purified on a silica column with $CHCl_3$ as eluant to give **3a** as a red powder (0.33 g, 82%). ^{1}H NMR (300 MHz, $CDCl_3$) δ 8.48–8.42 (m, 1H), 8.33–7.62 (m, 1H), 7.24 (dd, $J = 14.1$, 5.7 Hz, 4H), 7.09 (d, $J = 8.3$ Hz, 2H), 6.95–6.83 (m, 8H), 3.98 (q, $J = 6.4$ Hz, 4H), 3.10 (dd, $J = 62.0$, 13.0 Hz, 2H), 1.78 (dd, $J = 14.5$, 6.8 Hz, 4H), 1.52 (dd, $J = 14.9$, 7.4 Hz, 6H), 0.99 (td, $J = 7.3$, 2.5 Hz, 6H). Mass spectrum: *m*/*z* (EI): 543.1522 (M^++Na^+).

2.1.3. Poly(trans-bis(tributoxyphosphine)platinum(II)–N,N′-bis(4-n-butylbenzene)(2,6-bis-(ethynyl)anthraquinone diimine), *P2*

A 51.2 mg quantity (0.2 mmol) of **3a**, 134 mg (0.2 mmol) of *trans*-$Pt(PBu_3)_2Cl_2$, and 1.91 mg of CuI were dissolved in THF (50 mL) and Et_3N (50 mL), and the reaction was stirred at 65 °C for 48 h under N_2. The solvent was then evaporated, and the residue was purified by column chromatography using CH_2Cl_2/hexane (1:1, v/v) as the eluent to give **P2** (153 mg, 89%) as a red solid. ^{31}P NMR ($CDCl_3$): 3.22 ppm. ^{1}H NMR (300 MHz, $CDCl_3$) δ 8.16 (m, 1H), 7.39 (m, 1H), 7.13 (m, 1H), 6.88 (m, $J = 17.5$ Hz, 8H), 3.96 (s, 3H), 2.04 (d, $J = 41.5$ Hz, 9H), 1.78 (s, 4H), 1.69–1.21 (m, 23H), 0.94 (ddd, $J = 18.5$, 13.3, 6.8 Hz, 18H).

2.1.4. Instruments

^{1}H Nuclear Magnetic Resonance (NMR) spectra were recorded on a Bruker Avance 300 Ultrashield NMR spectrometer. Solid state UV–vis spectra were recorded on a Varian Cary 50 spectrophotometer at 298 K using raised-angle transmittance apparatus. Steady state emission and excitation spectra were measured on Edinburgh Instruments FLS980 Phosphorimeter equipped with single monochromators. The steady state emission spectra were recorded using an NMR tube for the 77 K measurements and an airtight 1 cm cuvette for measurements in solution at 298 K, which were prepared in a glove box. These spectra were corrected for instrument response. The phosphorescence lifetime measurements were performed with an Edinburgh Instruments FLS980 Phosphorimeter equipped with “flash” pulsed lamp. The frequency of the pulse was be adjusted from 1 to 100 Hz. All lifetime values were obtained from deconvolution and distribution lifetime analysis and multi-exponential analysis for comparison purposes. In addition, the molecular weight distributions of the polymers were determined by Waters 1515 GPC instrument with a Waters 1515 isocratic HPLC pump, a Waters 2414 refractive index detector and a waters 2998 photodiode array detector.

2.1.5. Film preparation

Solution of **P2** typically 10^{-3} M in CH_2Cl_2, were spun at 3000 rpm for 1 min with a spin coater from Speciality Coating System, 6800 Spin Coater Series.

2.1.6. Femtosecond transient absorption spectroscopy (fs-TAS)

The fs transient spectra and decay profiles were acquired on a homemade system using the SHG of a Soltice (Spectra Physics) Ti-

sapphire laser ($\lambda_{exc} = 398$ nm; fwhm = 75 fs; pulse energy = 0.1 μJ per pulse, rep. rate = 1 kHz; spot size ~ 500 μm), a white light continuum generated inside a sapphire window and a custom made dual CCD camera of 64 × 1024 pixels sensitive between 200 and 1100 nm (S7030, Spectronic Devices). The delay line permitted to probe up to 4 ns with an accuracy of ~4 fs. The results were analysed with the program Glotaran (http://glotaran.org) permitting to extract a sum of independent exponentials ($I(\lambda,t) = C_1(\lambda) \times e^{-\frac{t_1}{\tau}} + C_2(\lambda) \times e^{-\frac{t_2}{\tau}} + \cdots$) that fits the whole 3D transient map.

2.1.7. Fast kinetic emission decay measurements

The laser source was the same as described above. The IRF increased to a FWHM of ~9 ps after passing through the optics at 298 K and become 12 ps after passing through a Dewar for 77 K measurements. The detector was a Streak Camera (Axis-TRS, Axis Photonique Inc.) limited to a maximum of ~2.5 ns. The results were globally analysed with the program Glotaran (http://glotaran.org) permitting to extract a sum of independent exponentials ($I(\lambda, t) = C_1(\lambda) \bullet \exp(-t/\tau_1) + C_2(\lambda) \bullet \exp(-t/\tau_2) + \ldots$).

2.1.8. Computations

All density functional theory (DFT) and time dependent density functional theory (TD-DFT) calculations were performed with Gaussian 16 [43] at the Université de Sherbrooke with the Mammouth supercomputer supported by *Le Réseau Québécois De Calculs Hautes Performances*. The DFT geometry optimizations as well as TD-DFT calculations [44–52] were carried out using the B3LYP method. A 6–31 g* basis set was applied to C, H, N, and O atoms [53–58]. The VDZ (valence double ζ) with SBKJC effective core potentials were used for all Pt atoms [53–58]. All calculations were carried out in a THF solvent field. The calculated absorption spectra were obtained from GaussSum 3.0 [59].

2.1.9. Two-photon absorption

Two-photon absorption coefficient were obtained using a custom built open-aperture z-scan apparatus. The transmission of the fundamental at 795 nm at a repetition rate of 1 kHz and pulse duration of ~100 fs (Solstice, Spectra-Physics) were measured with a power-meter (1918-R, 918D-SL-OD3, Newport) as a function of z using a linear delay stage of 50 mm (UTM50PE.1, Newport). The resulting data were fitted using normalized transmittance for a purely two-photon absorption equation [60–62].

3. Results and discussion

*Synthesis of **P2***. **P2** was prepared in good overall yield (~66%) from the known starting materials 2,6-bis(trimethylsilylethynyl) anthracene-9,10-dione and 4-butoxyaniline (2 eqs.) according to Scheme 1. Their condensation using $TiCl_4$ as dehydrating agent in the presence of Dabco leads to compound **2a** in excellent isolated yield. Its subsequent deprotection by K_2CO_3 provides compound **3a**, also in good yield, which is then easily polymerized with the *trans*-$Pt(PBu_3)_2Cl_2$ complex in a 1:1 ratio in the presence of CuI and Et_3N to form the target organometallic polymer **P2**. The new compounds, **2a** and **3a**, and **P2** were characterized by ^1H and ^{31}P NMR, mass spectrometry and gel permeation chromatography (GPC). The polymer characteristics (average molecular weight in number (M_n), average molecular weight in weight (M_w), polydispersity (Đ) and degree of polymerisation (DP) are compared to those for **P0** and **P1** in Table 1. The polymer dimension increases going from **P0** → **P1** → **P2**. The latter increase (**P1** → **P2**) is most likely due to the effect of the soluble chain. The ^{31}P NMR spectrum exhibits a singlet resonance at 3.22 ppm (in $CDCl_3$) comparing favourably to that of **P1** (3.18 ppm, [38]).

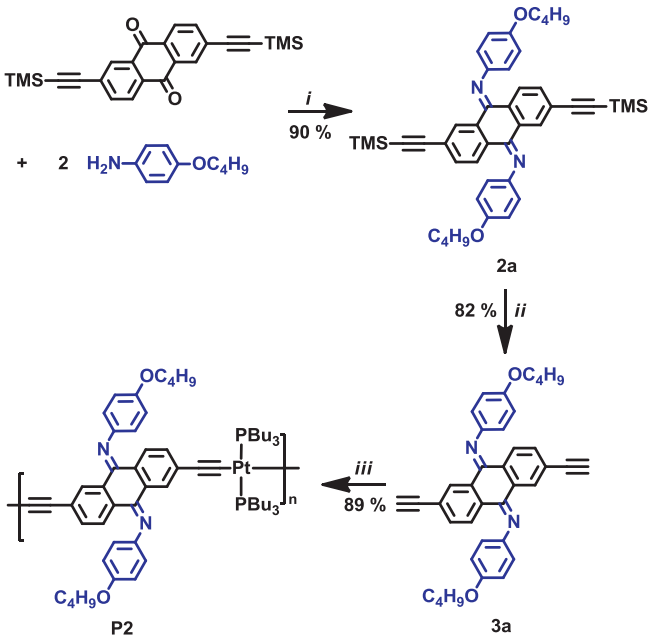

Scheme 1. Synthesis of **P2**: *i*) $TiCl_4$, Dabco, C_6H_5Cl, 115 °C; *ii*) K_2CO_3, THF/MeOH, R.T.; *iii*) *trans*-$Pt(PBu_3)_2Cl_2$, Et_3N, CuI, CH_2Cl_2, R.T.

3.1. Absorption properties

The absorption and fluorescence spectra of **P2** in 2MeTHF and in film at 298 K are presented in Fig. 2. The absorption spectrum is characterized by a maximum at ~390 nm and a long tail spreading from 430 to 600 nm. The interpretation of the absorption spectra and the low-energy emissive state S_1 was made using DFT and TDDFT computations using (HC≡C-**[Pt]**-(**AQI**(X)$_2$)-**[Pt]**-C≡CH) as model for **P2** (X = OBu). The HOMO-2, HOMO-1, HOMO and LUMO exhibit atomic contributions associated with π-systems spreading over the *trans*-$Pt(PMe)_2(C{\equiv}C)_2$, **AQI** and pendent $C_6H_4OC_4H_9$ groups (Fig. 3; see Supporting Information for more frontier MOs) and are expectedly reminiscent to that for **P1** (X = NO_2; [40]). The detail of the atomic contributions is provided and Table 2. A HOMO → LUMO transition generates a charge transfer (CT state) of the type [*trans*-$Pt(PMe)_2(C{\equiv}C)_2$]-to-**AQI**/C_6H_4X, somewhat similar to the common metal-to-ligand charge transfer state (MLCT).

TDDFT is employed to predict the positions and nature of the low-lying singlet excited states (Table 3, see Supporting Information for all 100th transitions). The calculated lowest-energy transitions are evidently shifted to the blue for **P2** when compared to **P1** [40], a behaviour anticipated with the withdrawing effect of the groups, NO_2, compared to the electron donating OBu's [63]. Using the calculated positions of the 100th transitions (Fig. 2, bottom, blue) one can simulate a spectrum by assigning an arbitrary FWHM of 1000 cm^{-1} (black line). The comparison with the experimental spectrum is good, particularly in the low-energy region.

Table 1
Comparison of the polymer characteristics (GPC).

Px [ref]	M_n	M_w	Đ	DP
P2 [tw]	147000	327000	2.23	133
P1 [38]	88200	188700	2.14	111
P0 [37]	26300	80300	3.06	31

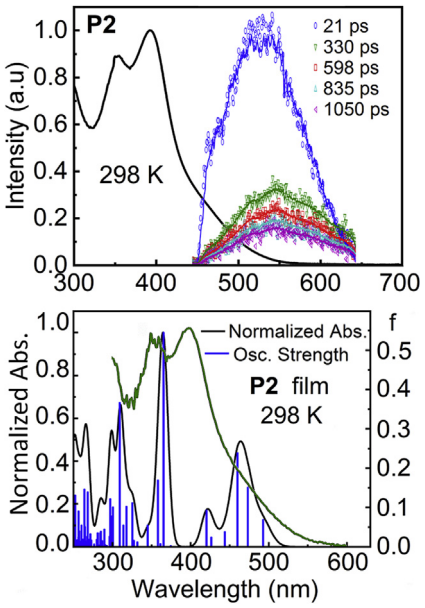

Fig. 2. Top: absorption (black; $\varepsilon = 17000$ (352), 19700 $M^{-1}\,cm^{-1}$ (394 nm)) and time-resolved fluorescence spectra (in colours: delay times indicated inside the frame, using a Streak camera) of **P2** in 2MeTHF at 298 K, $\lambda_{exc} = 397$ nm (for the 77 K data, see Supporting Information). Bottom: comparison of the absorption (green) of **P2** as film and a bar graph (blue) reporting the calculated oscillator strength (f) and calculated positions of the 100th electronic transitions for the (HC≡C-**[Pt]**-(**AQI**$(OBu)_2$)-**[Pt]**-C≡CH) model (TDDFT). The black line is generated by assigning an arbitrary FWHM of 1000 cm^{-1} to each transition. (For interpretation of the references to colour in this figure legend, the reader is referred to the Web version of this article.)

3.2. Fluorescence properties

P2 is fluorescent with a λ_{max} ~ 545 nm. This emission band is also flanked with a shoulder near 470 nm (Fig. 2, top), which decays rapidly in the time-resolved spectra. In comparison with **P1** [40], the fluorescence intensity of **P2** is more intense based on the qualitative signal-to-noise ratio. This conclusion is perfectly in line with the significantly longer S_1 lifetimes for **P2** compared to **P1** (Table 4). The decay associated spectra reveals the presence of three components (Fig. 4). The shoulder now appears as a well-defined band at ~485 nm with a lifetime of ≤11.4 ps (i.e. the limit of the IRF). This component correspond to an upper S_n excited state (also observed on the fs-TAS), which is readily deduced by the typical S-shape of the decay associated spectrum of this component (positive response = upper S_n = energy donor and negative response = S_1 = energy acceptor).

The remainder species ($\lambda_{max} = 545$ nm, green; $\lambda_{max} = 550$ nm, red) are most likely the terminal and central units, respectively, based upon their relative position (the end groups are always blue-shifted due to a lesser extend of the conjugation) common in **[Pt]**-containing polymers [64,65]. The fluorescence lifetimes (τ_F) show one order a magnitude difference associated from the upper-energy excited state (terminal) to the lower one (central). The rate for singlet-singlet energy transfer, k_{ET}, is given by $k_{ET} = (1/\tau_F) - (1/\tau_F^{\circ})$, where τ_F and τ_F° are the fluorescence lifetimes of the donor in the presence and absence of energy transfer, here the short and long lifetimes, respectively (since the chromophores are the same). Using the data in Table 4, k_{ET} ~$1 \times 10^{10}\ s^{-1}$ at both temperatures. This value is considered typical for a singlet-singlet energy transfer and on the fast side. The fact that k_{ET} is weakly temperature-

Table 2
Relative atomic contributions (%) of the various fragments to the frontier MOs of optimized (HC≡C-**[Pt]**-(**AQI**$(X)_2$)-**[Pt]**-C≡CH) models (X = OBu, **P2**; NO_2, **P1** [38]).

Fragments **P2**	HOMO-2	HOMO-1	HOMO	LUMO
[Pt(PBu_3)$_2$]	16.9	31.8	29.9	7.2
(C≡C)+(C≡CH)	17.3	37.0	36.0	3.2
AQI: ($C_{14}H_6N_2$)	30.1	23.9	27.2	74.7
($C_6H_4OC_4H_9$)	35.6	7.4	7.0	15.0
Fragments **P1** [38]	HOMO-2	HOMO-1	HOMO	LUMO
[Pt(PBu_3)$_2$]	35.0	39.9	32.6	1.4
(C≡C)+(C≡CH)	47.5	46.9	42.3	2.3
AQI: ($C_{14}H_6N_2$)	16.4	12.4	23.4	58.8
($C_6H_4OC_4H_9$)	1.1	0.7	1.7	37.6

Table 3
Calculated position, oscillator strength (f) and major contributions (%) of the first 100 singlet-singlet electronic transitions of optimized (HC≡C-**[Pt]**-(**AQI**$(X)_2$)-**[Pt]**-C≡CH) models (X = OBu, **P2**; NO_2, **P1** [40]).

No.	λ (nm)	f	Major contributions (%) for P2
1	492.8	0.069	H-2→LUMO (19), HOMO→LUMO (71)
2	473.2	0.151	H-2→LUMO (38), H-1→LUMO (31), HOMO→LUMO (11)
3	460.0	0.239	H-2→LUMO (24), H-1→LUMO (60), HOMO→LUMO (12)
No.	λ (nm)	f	Major contributions (%) for P1 (from Ref. [38])
1	526.9	0.015	HOMO→LUMO (96)
2	514.4	0.091	H-1→LUMO (96)
3	492.0	0.051	H-2→LUMO (87)

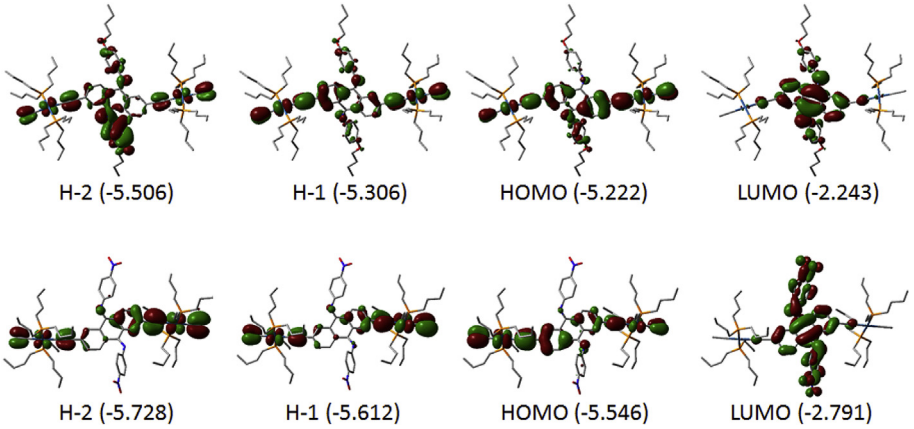

Fig. 3. Representations of the frontier MOs for of optimized (HC≡C-**[Pt]**-(**AQI**$(X)_2$)-**[Pt]**-C≡CH) models (X = OBu, **P2**). The case where X = NO_2, **P1** ([38]) is provided for comparison purposes and convenience.

Table 4
Comparison of the photophysical data of **P0**, **P1** and **P2** (in 2MeTHF).

Px [ref]	λ_F (nm)	τ_F (ps)	λ_P (nm)	τ_P (μs)
P2 [tw][a]	545 (298 K)[b]	79 and 834	–	–
	545 (77 K)	99 and 1200	–	–
P1 [38]	550 (298 K)[b]	11	–	–
	550 (77 K)	26	–	–
P0 [37]	–	–	585 (77 K)	273

[a] tw = this work.
[b] $\Phi_F < 0.001$, which is below the detection limit.

dependent is also normal, unlike the electron transfer. The reason why such a common phenomenon was not detected in **P1** most probably stem from its rather low fluorescence intensity and short S_1 lifetimes (*i.e.* 11 ps at 298 K [40], which is close to the detection limit, IRF).

3.3. Fs-transient absorption response

The very short-lived fluorescence component of **P2** (*i.e.* ≤ 11.4 ps) was also detected in the fs-TAS measurements, here with a value of 12.4 ps (in 2MeTHF) and of 6.5 ps (as a film, Fig. 5).

The longer-lived ps-ns species described above were not detected in 2MeTHF, most likely as the resulting traces may be too weak to be detected (see the red and green traces, which are already weak, Fig. 5, top). However a component of 3.3 ns (green trace), which exhibits a different signature compared to 6.5 ps-component (red line, Fig. 5, bottom) has been detected for **P2** studied as a film. Finally, the comparison of the three components for **P2** in 2MeTHF (<100 fs (IRF limit), 766 fs, 12.4 ps (all three components are attributable to upper S_n species); Fig. 5, top right) compares favorably to that reported for **P1** (139 fs, 1.1 ps and 11.5 ps [40]). The two shorter-lived species ((<100 fs, 766 fs) are also upper energy S_n species decaying in the fs time scale as $\lambda_{exc} = 397$ nm, which permits their population (see TDDFT data in Fig. 2 (bottom) and Table 2).

3.4. Triplet states

No emission attributable to a T_1 emission has been detected above 600 nm (*i.e.* at longer wavelength of the S_1 fluorescence). The absence of phosphorescence is common for this class of *push-pull* materials [10,39,63]. For sake of convenience, the nature of this non-emissive excited state (T_1) was also addressed by DFT computations. The results are placed in the Supporting Information and include MO representations of the low semi-occupied and high semi-occupied MOs (respectively LSOMO and HSOMO) as well as the relative atomic contributions of the various fragments to these MOs of optimized (HC≡C-**[Pt]**-(**AQI**(OBu)$_2$)-**[Pt]**-C≡CH) model. The conclusion is that this T_1 state is also predicted to be of the same nature of the S_1 state: [*trans*-Pt(PMe)$_2$(C≡C)$_2$]-to-**AQI**/C_6H_4OBu.

Concurrently, an upper T_n emission is detected at 460 nm for **P2** at 77 K only using a steady state set-up (Fig. 6). The spectra signature is unambiguously associated with a localized triplet state of the [*trans*-Pt(PMe)$_2$(C≡C)$_2$] moiety, which again is common in this type of organometallic polymers [10]. This signal is not detected by the Streak camera because it emission decay exceeds the temporal detection limit of the Streak camera (~3 ns). This signal decays in the μs time scale, which is characteristic for a triplet emission (Table 5). The signal is multi-exponential and this behaviour cannot be attributed to an energy transfer (terminal *vs.* central) because this emission is known to be localized onto the [*trans*-Pt(PMe)$_2$(C≡C)$_2$] moiety. Instead, the multi-exponential behaviour of this type of chromophore as a single complex, whether it is in solution or in the solid state, has recently been addressed in detail [66]. These different lifetimes results from the various conformers that may exist upon the dihedral angle made by the [*trans*-Pt(PMe)$_2$(C≡C)$_2$] plane and that for the aromatic side groups. We propose that a similar situation occur here. Note that the corresponding T_1 emission for **P1** was not investigated in the earlier investigation, since it was not the goal of this earlier work.

3.1. Two-photon absorption

The two-photon absorption (2 PA) cross sections (σ_2) for the **P1** and **P2** in THF were obtained using an open aperture Z-scan technique [61,62] and the experiments were conducted at $\lambda_{exc} = 795$ nm (Fig. 7). The 2 PA results are presented and compared with other **[Pt]**-containing polymers in Table 6.

According to the Z-scan results, the σ_2 range from 53 to 89 GM (Gøppert-Mayer; 1 GM = 10^{-50} cm^4 s/photon)) at the intensities of the input pulse between 252 and 327 GW/cm^2 respectively for **P1**, whereas **P2** exhibits σ_2 values ranging from 45 to 70 GM with intensities of the input pulse between 252 and 327 GW/cm^2, respectively, assuming that only 2 PA is occurring. While **P1** appears to have a slightly better σ_2 value than that for **P2**, and somewhat similar to another [Pt]-containing polymer (i.e. (**[Pt]**-T-CBZ-T)$_n$; T = thiophene; CBZ = 3,3′-carbazole) [67], these σ_2 data are a little modest in comparison with those reported for other related [Pt]-containing polymers in the literature where the 2 PA cross sections are found between 10 and 280 GM [68]. Because the experimental conditions differ from one investigation to another, and that the polymer dimensions are also different, no reliable structure-properties can be provided at the moment.

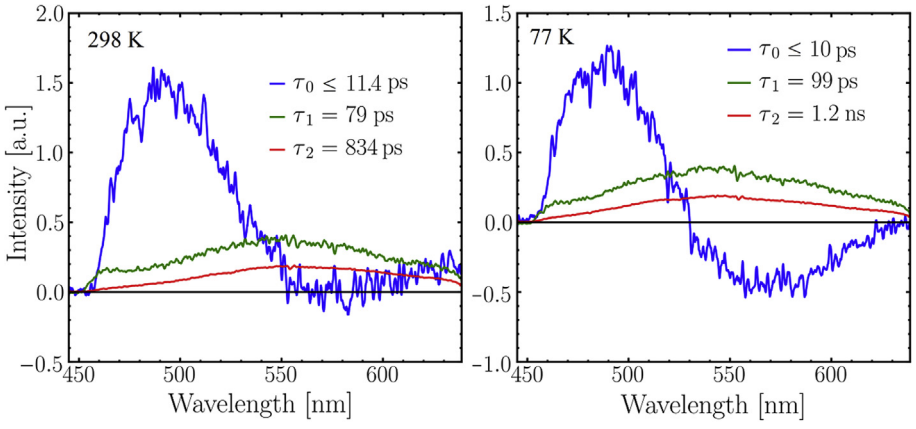

Fig. 4. Decay associated spectra of **P2** in 2MeTHF at 298 and 77 K showing the three components of the time-resolved spectra.

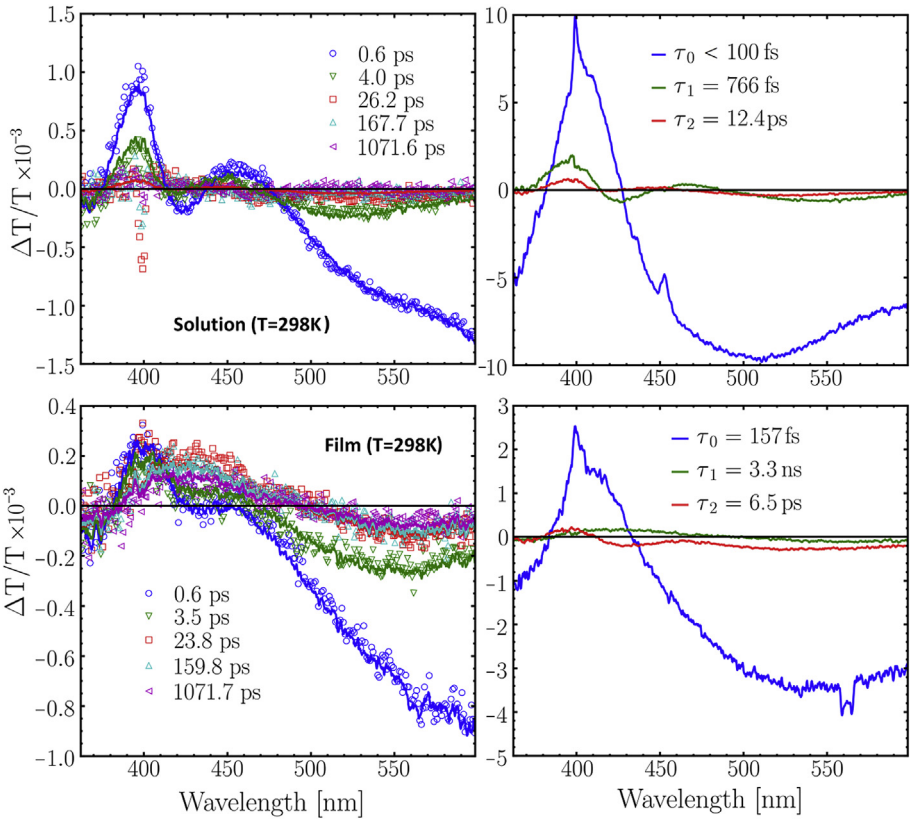

Fig. 5. Left: Time evolution of the fs-TAS of **P2** in 2MeTHF (top) and as a film (bottom), $\lambda_{exc} = 397$ nm (IRF = 100 fs). Right: decay associated spectra of **P2** in 2MeTHF (top) and as a film (bottom) showing three components. The bleach and transient signals are the positive and negative signals, respectively.

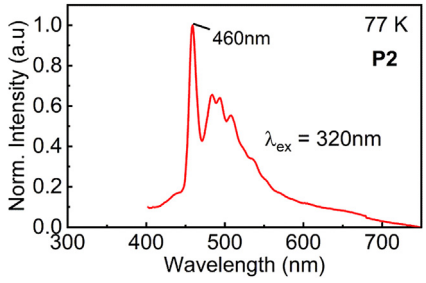

Fig. 6. Emission spectrum for **P2** at 77 K in 2MeTHF using a steady state instrument. The fluorescence band is barely detected under this signal in the 500–700 nm window.

Table 5
τ_e data for **P2** at 77 K in 2MeTHF (B_i = pre-exponential factor).

Comp.	λ_{em}(nm)	B_i	τ_e; μs (f in %)[a]	χ^2
P2	460	0.2732	0.65 (12)	1.021
		0.0011	18.3 (1)[b]	
		0.0112	120 (87)	

[a] $f_i(\%) = (B_i\tau_i)/\Sigma(B_i\tau_i) \bullet 100\%$; $I_e(t) = B_1\exp(-t/\tau_1) + B_2\exp(-t/\tau_2) + B_3\exp(-t/\tau_3) + \ldots$
[b] With 1% of contribution, this component is most likely not accurate.

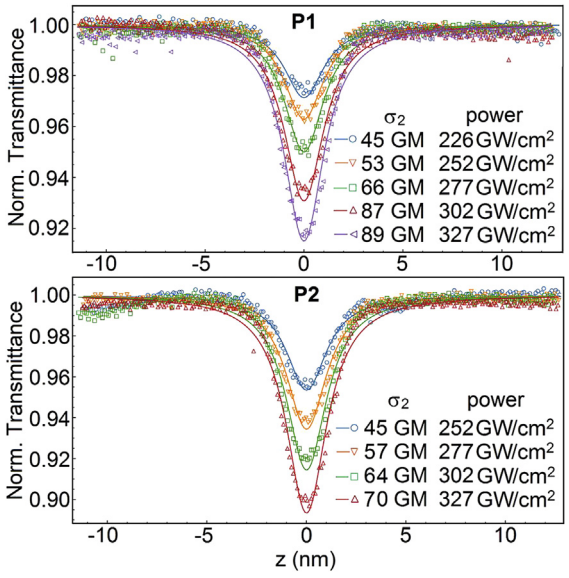

Fig. 7. Z-scan results for **P1** (top) and **P2** (bottom) in THF solvent. The open symbols in the figure indicate the experimental measured transmission data and the 'solid lines' are obtained by fitting the experimental data to the 2 PA equation. The σ_2 data and the different input powers are provided.

4. Conclusion

This comparative study showed significant differences in physical properties between **P0**, **P1** and **P2**. First, the polymer dimensions of **P2** is larger than that for **P1** (and **P0**) due to the presence of soluble chains (-OC_4H_9) instead of NO_2 groups, but unexpectedly **P2** exhibits a higher fluorescence intensity and lifetime than that for **P1**, which is counter-intuitive due to the "loose bolt effect" of side alkyl chains. Second, **P2** exhibits a rare case of higher energy emission associated with an upper S_n excited state,

Table 6
2-Photon absorption data for **P1** and **P2**.[a]

Polymer[b]	Ref.	σ_2 (GM)	λ_{exc} (nm)
P1 (**[Pt]**-AQI$(NO_2)_2)_n$	tw	53–89	795
P2 (**[Pt]**-AQI$(OC_4H_9)_2)_n$	tw	45–70	795
(**[Pt]**-T-CBZ-T)$_n$	67	10–100	600
(**[Pt]**-C_6H_4-O*x*-$C_6H_4)_n$	68	175	730
(**[Pt]**-F-O*x*-F)$_n$	68	280	730
((**[Pt]**-(F-Q*x*)$_2$-F))$_n$	68	260	730

[a] tw = this work. In THF, [**P1**] = 0.37 mM, [**P2**] = 0.54 mM. b) T = 1,1′- thiophene, CBZ = 3,3′- carborzole, O*x* = oxadiazole, F = 2,2′-fluorene.

which is not observed in **P1**. These observations suggest that the incorporation of the soluble side chains on conjugated polymers in order to change the morphology of the resulting photoactive nanofilm in bulk heterojunction solar cells may not necessarily be detrimental to the excited state properties, notably the excited state lifetimes prior to the photo-induced electron transfer. Concurrently, **P0** is only phosphorescent (T_1), while **P1** and **P2** are not emissive from the T_1 state, thus stressing the drastic substitution effect going from = O to = N–C_6H_4-X, and also from X = NO_2 to OC_4H_9.

Acknowledgment

This research was supported by the Natural Sciences and Engineering Research Council of Canada (NSERC).

Appendix A. Supplementary data

Supplementary data to this article can be found online at https://doi.org/10.1016/j.jorganchem.2019.05.024.

References

[1] C.L. Ho, Z.Q. Yu, W.Y. Wong, Multifunctional polymetallaynes: properties, functions and applications, Chem. Soc. Rev. 45 (2016) 5264–5295.
[2] J. Xiang, C.L. Ho, W.Y. Wong, Metallopolymers for energy production, storage and conservation, Polym. Chem. 6 (2015) 6905–6930.
[3] L. Ying, C.L. Ho, H. Wu, Y. Cao, W.Y. Wong, White polymer light-emitting devices for solid-state lighting: materials, devices, and recent progress, Adv. Mater. 26 (2014) 2459–2473.
[4] X. Yang, G. Zhou, W.Y. Wong, Recent design tactics for high performance white polymer light-emitting diodes, J. Mater. Chem. C 2 (2014) 1760–1778.
[5] C.L. Ho, W.Y. Wong, Heavy-metal organometallic complexes as yellow and orange triplet emitters for organic light-emitting diodes, in: Molecular Design and Applications of Photofunctional Polymers and Materials, 2012, pp. 1–30.
[6] C.L. Ho, W.Y. Wong, Charge and energy transfers in functional metallophosphors and metallopolyynes, Coord. Chem. Rev. 257 (2013) 1614–1649.
[7] C.L. Ho, W.Y. Wong, Metal-containing polymers: facile tuning of photophysical traits and emerging applications in organic electronics and photonics, Coord. Chem. Rev. 255 (2011) 2469–2502.
[8] W.Y. Wong, Optical properties and photophysics of Platinum–Containing poly (aryleneethynylene)s, Macromolecules Containing Metal and Metal-Like Elements: Photophycics. Photochem. Metal-Containing Polymers 10 (2010) 289–324.
[9] W. Zheng, W. Wang, S.T. Jiang, G. Yang, Z. Li, X.Q. Wang, G.Q. Yin, Y. Zhang, H. Tan, X. Li, H. Ding, Supramolecular transformation of metallacycle-linked star polymers driven by simple phosphine ligand-exchange reaction, J. Am. Chem. Soc. 141 (2019) 583–591.
[10] P.D. Harvey, Organometallic and coordination polymers, and linear and star oligomers using the *trans*-Pt$(PR_3)_2(C\equiv C)_2$ linker, J. Inorg. Organomet. Polym. Mater. 27 (2017) 3–38.
[11] Y. Miyagi, T. Ishida, M. Marumoto, N. Sano, T. Yajima, F. Sanda, Ligand exchange reaction for controlling the conformation of platinum-containing polymers, Macromolecules 51 (2018) 815–824.
[12] A. Lapprand, N. Khiri, D. Fortin, S. Jugé, P.D. Harvey, Organometallic oligomers based on bis (arylacetylide) bis (p-chirogenic phosphine) platinum (II) complexes: synthesis and photonic properties, Inorg. Chem. 52 (2013) 2361–2371.
[13] J.S. Dhindsa, R.R. Maar, S.M. Barbon, M.O. Avilés, Z.K. Powell, F. Lagugné-Labarthet, J.B. Gilroy, A π-conjugated inorganic polymer constructed from boron difluoride formazanates and platinum (ii) diynes, Chem. Commun. 54 (2018) 6899–6902.
[14] X. Wang, Y. Han, Y. Liu, G. Zou, Z. Gao, F. Wang, Cooperative supramolecular polymerization of fluorescent platinum acetylides for optical waveguide applications, Angew. Chem. 129 (2017) 12640–12644.
[15] C. Chakraborty, R.K. Pandey, U. Rana, M. Kanao, S. Moriyama, M. Higuchi, Geometrically isomeric Pt (II)/Fe (II)-based heterometallo-supramolecular polymers with organometallic ligands for electrochromism and the electrochemical switching of Raman scattering, J. Mater. Chem. C 4 (2016) 9428–9437.
[16] S. Cekli, R.W. Winkel, K.S. Schanze, Effect of oligomer length on photophysical properties of platinum acetylide donor–acceptor–donor oligomers, J. Phys. Chem. A 120 (2016) 5512–5521.
[17] Y. Miyagi, Y. Shibutani, Y. Otaki, F. Sanda, Synthesis of platinum-containing poly (phenyleneethynylene)s having various chromophores: aggregation and optical properties, Polym. Chem. 7 (2016) 1070–1078.
[18] K. Wei, Z. Gao, H. Liu, X. Wu, F. Wang, H. Xu, Mechanical activation of platinum–acetylide complex for olefin hydrosilylation, ACS Macro Lett. 6 (2017) 1146–1150.
[19] Y. Du, N. Dong, M. Zhang, B. Jiang, N. Sun, Y. Luo, S. Zhang, G. Wang, J. Wang, Poly (arylene ether)s based on platinum (II) acetylide complexes: synthesis and photophysical and nonlinear absorption properties, J. Mater. Chem. C 6 (2018) 7317–7325.
[20] D. Chateau, A. Liotta, H. Lundén, F. Lerouge, F. Chaput, D. Krein, T. Cooper, C. Lopes, A.A. El-Amay, M. Lindgren, et al., Long distance enhancement of nonlinear optical properties using low concentration of plasmonic nanostructures in dye doped monolithic sol–gel materials, Adv. Funct. Mater. 26 (2016) 6005–6014.
[21] R.S. Price, G. Dubinina, G. Wicks, M. Drobizhev, A. Rebane, K.S. Schanze, Polymer monoliths containing two-photon absorbing phenylenevinylene platinum (II) acetylide chromophores for optical power limiting, ACS Appl. Mater. Interfaces 7 (2015) 10795–10805.
[22] S. Goswami, G. Wicks, A. Rebane, K.S. Schanze, Photophysics and non-linear absorption of Au (I) and Pt (II) acetylide complexes of a thienyl-carbazole chromophore, Dalton Trans. 43 (2014) 17721–17728.
[23] A. Colombo, F. Nisic, C. Dragonetti, D. Marinotto, I.P. Oliveri, S. Righetto, M.G. Lobello, F. De Angelis, Unexpectedly high second-order nonlinear optical properties of simple Ru and Pt alkynyl complexes as an analytical springboard for NLO-active polymer films, Chem. Commun. 50 (2014) 7986–7989.
[24] A.H. Shelton, R.S. Price, L. Brokmann, B. Dettlaff, K.S. Schanze, High efficiency platinum acetylide nonlinear absorption chromophores covalently linked to poly (methyl methacrylate), ACS Appl. Mater. Interfaces 5 (2013) 7867–7874.
[25] C.L. Ho, C.H. Chui, W.Y. Wong, S.M. Aly, D. Fortin, P.D. Harvey, B. Yao, Z. Xie, L. Wang, Efficient electrophosphorescence from a platinum metallopolyyne featuring a 2, 7-carbazole chromophore, Macromol. Chem. Phys. 210 (2009) 1786–1798.
[26] W. He, M.Y. Livshits, D.A. Dickie, Z. Zhang, L.E. Mejiaortega, J.J. Rack, Q. Wu, Y. Qin, "Roller-Wheel"-Type Pt-containing small molecules and the impact of "rollers" on material crystallinity, electronic properties, and solar cell performance, J. Am. Chem. Soc. 139 (2017) 14109–14119.
[27] W. He, M.Y. Livshits, D.A. Dickie, J. Yang, R. Quinnett, J.J. Rack, Q. Wu, Y. Qin, A "roller-wheel" Pt-containing small molecule that outperforms its polymer analogs in organic solar cells, Chem. Sci. 7 (2016) 5798–5804.
[28] L. Li, X.X. Sun, Y. Hu, Q.H. Wu, Synthesis of a new platinum metallopolyyne for organic solar cells, in: Advanced Materials Research, vol. 430, Trans Tech Publications, 2012, pp. 260–263.
[29] H. Zhan, S. Lamare, A. Ng, T. Kenny, H. Guernon, W.K. Chan, A.B. Djurisic, P.D. Harvey, W.Y. Wong, Synthesis and photovoltaic properties of new metalloporphyrin-containing polyplatinyne polymers, Macromolecules 44 (2011) 5155–5167.
[30] Q. Wang, Z. He, A. Wild, H. Wu, Y. Cao, U.S. Schubert, C.H. Chui, W.Y. Wong, Platinum–acetylide polymers with higher dimensionality for organic solar cells, Chem. Asian J. 6 (2011) 1766–1777.
[31] L. Li, W.C. Chow, W.Y. Wong, C.H. Chui, R.S.M. Wong, Synthesis, characterization and photovoltaic behavior of platinum acetylide polymers with electron-deficient 9, 10-anthraquinone moiety, J. Organomet. Chem. 696 (2011) 1189–1197.
[32] Q. Wang, W.Y. Wong, New low-bandgap polymetallaynes of platinum functionalized with a triphenylamine-benzothiadiazole donor–acceptor unit for solar cell applications, Polym. Chem. 2 (2011) 432–440.
[33] W.Y. Wong, W.C. Chow, K.Y. Cheung, M.K. Fung, A.B. Djurišić, W.K. Chan, Harvesting solar energy using conjugated metallopolyyne donors containing electron-rich phenothiazine–oligothiophene moieties, J. Organomet. Chem. 694 (2009) 2717–2726.
[34] J. Mei, K. Ogawa, Y.G. Kim, N.C. Heston, D.J. Arenas, Z. Nasrollahi, T.D. McCarley, D.B. Tanner, J.R. Reynolds, K.S. Schanze, Low-band-gap platinum acetylide polymers as active materials for organic solar cells, ACS Appl. Mater. Interfaces 1 (2009) 150–161.
[35] L. Liu, C.L. Ho, W.Y. Wong, K.Y. Cheung, M.K. Fung, W.T. Lam, A.B. Djurišić, W.K. Chan, Effect of oligothienyl chain length on tuning the solar cell performance in fluorene-based polyplatinynes, Adv. Funct. Mater. 18 (2008) 2824–2833.
[36] L. Xu, C.L. Ho, L. Liu, W.Y. Wong, Molecular/polymeric metallaynes and related molecules: solar cell materials and devices, Coord. Chem. Rev. 373 (2018) 233–257.
[37] W.Y. Wong, C.L. Ho, Organometallic photovoltaics: a new and versatile approach for harvesting solar energy using conjugated polymetallaynes, Acc.

Chem. Res. 43 (2010) 1246–1256.
[38] A. Bonnot, P.D. Harvey, Pentacene-and BODIPY-Containing trans-Bis (ethynyl) bis (phosphine) platinum (II) Organometallic Polymers: a DFT Point of View, J. Inorg. Organomet. Polym. Mater. 26 (2016) 1328–1337.
[39] X. Wang, D. Fortin, G. Brisard, P.D. Harvey, Drastic tuning of the photonic properties of «(Push–Pull) n» *trans*-bis (ethynyl) bis (tributylphosphine) platinum (II)-Containing polymers, Macromol. Rapid Commun. 35 (2014) 992–997.
[40] H. Lei, F. Juvenal, P.L. Karsenti, D. Fortin, P.D. Harvey, Cross conjugated organometallic polymers exhibiting ultrafast excitation energy channeling: drastic effect of the connectivity, Macromol. Chem. Phys. 219 (2018) 1800354.
[41] G.B. Kauffman, L.A. Teter, J.E. Huheey, *cis*-and *trans*-Dichlorobis (tri-n-butylphosphine) platinum (II), Inorg. Synth. 7 (1963) 245–249.
[42] X. Wang, D. Fortin, G. Brisard, P.D. Harvey, Drastic tuning of the photonic properties of «(Push–Pull) n» trans-bis (ethynyl) bis (tributylphosphine) platinum (II)-Containing polymers, Macromol. Rapid Commun. 35 (2014) 992–997.
[43] M.J. Frisch, G.W. Trucks, H.B. Schlegel, G.E. Scuseria, M.A. Robb, J.R. Cheeseman, J.A. Montgomery, T. Vreven, K.N. Kudin, J.C. Burant, J.M. Millam, et al., Gaussian 16, Gaussian, Inc., Wallingford, CT, 2016.
[44] P. Hohenberg, W. Kohn, The inhomogeneous electron gas, Phys. Rev. 136 (1964) B864–B871.
[45] P. Hohenberg, L.J. Sham, Self-consistent equations including exchange and correlation effects, J. Phys. Rev. 140 (1965) 1133–1138.
[46] C. Lee, W. Yang, R.G. Parr, Development of the Colic-Salvetti correlation-energy formula into a functional of the electron density, Phys. Rev. B 37 (1988) 785–789.
[47] B. Miehlich, A. Savin A, H. Stoll, H. Preuss, Results obtained with the correlation energy density functionals of Becke and Lee, Yang and Parr, Chem. Phys. Lett. 157 (1989) 200–206.
[48] R.G. Parr, W. Yang, Density functional theory of atoms and molecules, Int. J. Quantum Chem. 47 (1989) 101.
[49] A.D. Becke, Density-functional thermochemistry. III. The role of exact exchange, J. Chern. Phys. 98 (1993) 5648–5652.
[50] R. Bauernschmitt, R. Ahlrichs, Treatment of electronic excitations within the adiabatic approximation of time dependent density functional theory, Chem. Phys. Lett. 256 (1996) 454–464.
[51] M.E. Casida, C. Jamorski, K.C. Casida, D.R. Salahub, Molecular excitation energies to high-lying bound states from time-dependent density- functional response theory : characterization and correction of the time-dependent local density approximation ionization threshold, J. Chem. Phys. 108 (1998) 4439–4449.
[52] R.E. Stratmann, G.E. Scuseria, M.J. Frisch, An efficient implementation of time-dependent density-functional theory for the calculation of excitation energies of large, J. Chem. Phys. 109 (1998) 8218–8224.
[53] J.S. Binkley, J.A. People, W.J. Hehre, Self-consistent molecular orbital methods. 21. Small split-valence basis sets for first-row elements, J. Am. Chem. Soc. 102 (1980) 939–947.
[54] M.S. Gordon, J.S. Binkley, J.A. Pople, W.J. Pietro, W.J. Hehre, Self-consistent molecular-orbital methods. 22. Small split-valence basis sets for second-row elements, J. Am. Chem. Soc. 104 (1982) 2797–2803.
[55] W.J. Pietro, M.M. Francl, W.J. Hehre, D.J. Defrees, J.A. People, J.S. Binkley, Self-consistent molecular orbital methods. 24. Supplemented small split-valence basis sets for second-row elements, J. Am. Chem. Soc. 104 (1982) 5039–5048.
[56] K.D. Dobbs, W.J. Hehre, Molecular orbital theory of the properties of inorganic and organometallic compounds 4. Extended basis sets for third-and fourth-row, main-group elements, J. Comput. Chem. 7 (1986) 359–378.
[57] K. Dobbs, W. Hehre, Molecular-orbital theory of the properties of inorganic and organometallic compounds. 5. Extended basis-sets for 1st-row transition-metals, J. Comput. Chem. 8 (1987) 861–879.
[58] K.D. Dobbs, W.J. Hehre, Molecular orbital theory of the properties of inorganic and organometallic compounds. 6. Extended basis sets for second-row transition metals, J. Comput. Chem. 8 (1987) 880–893.
[59] N.M.O. Boyle, A.L. Tenderholt, K.M. Langner, Software news and updates cclib : a library for package-independent computational Chemistry algorithms, J. Comput. Chem. 29 (2007) 839–845.
[60] B.A. Reinhardt, Two-photon technology: new materials and evolving applications, Photon. Sci. News 4 (1999) 21–33.
[61] A. Ajami, M.S. Rafique, N. Pucher, S. Bashir, W. Husinsky, R. Liska, R. Inführ, H. Lichtenegger, J. Stampfl, December, Z-scan measurements of two-photon absorption for ultrashort laser radiation, in: 15th International School on Quantum Electronics: Laser Physics and Applications, International Society for Optics and Photonics, 2008, p. 7027, 70271H.
[62] I.C. Khoo, S. Webster, S. Kubo, W.J. Youngblood, J.D. Liou, T.E. Mallouk, P. Lin, D.J. Hagan, E.W. Van Stryland, Synthesis and characterization of the multi-photon absorption and excited-state properties of a neat liquid 4-propyl 4′-butyl diphenyl acetylene, J. Mater. Chem. 19 (2009) 7525–7531.
[63] T. Kenny, S.M. Aly, G. Brisard, D. Fortin, P.D. Harvey, The Pt-organometallic version of perigraniline: going blue, Macromol. Rapid Commun. 34 (2013) 511–515.
[64] A.M. Soliman, D. Fortin, E. Zysman-Colman, P.D. Harvey, Unexpected evolution of optical properties in Ir–Pt complexes upon repeat unit increase: towards an understanding of the photophysical behaviour of organometallic polymers, Chem. Commun. 48 (2012) 6271–6273.
[65] S. Clement, T. Goudreault, D. Bellows, D. Fortin, L. Guyard, M. Knorr, P.D. Harvey, Probing excited state electronic communications across diethynyl-[2.2] paracyclophane-containing conjugated organometallic polymers, Chem. Commun. 48 (2012) 8640–8642.
[66] G. Marineau-Plante, F. Juvenal, A. Langlois, D. Fortin, A. Soldera, P.D. Harvey, Multiply "trapped" ^{3}[*trans*-Pt$(PR_3)_2(C{\equiv}CC_6H_4X)_2$]* conformers in rigid media, Chem. Commun. 54 (2018) 976–979.
[67] S. Goswami, G. Wicks, A. Rebane, K.S. Schanze, Photophysics and non-linear absorption of Au (I) and Pt (II) acetylide complexes of a thienyl-carbazole chromophore, Dalton Trans. 43 (2014) 17721–17728.
[68] T. Goudreault, Z. He, Y. Guo, C.L. Ho, H. Zhan, Q. Wang, K.Y.F. Ho, K.L. Wong, D. Fortin, B. Yao, Z. Xie, Synthesis, light-emitting, and two-photon absorption properties of platinum-containing poly(arylene-ethynylene)s linked by 1, 3, 4-oxadiazole units, Macromolecules 43 (2010) 7936–7949.